NASA Technical Memorandum 4416

Flight-Determined Stability Analysis of Multiple-Input–Multiple-Output Control Systems

John J. Burken
Dryden Flight Research Facility
Edwards, California

National Aeronautics and Space Administration

Office of Management

Scientific and Technical Information Program

1992

FLIGHT-DETERMINED STABILITY ANALYSIS OF MULTIPLE-INPUT–MULTIPLE-OUTPUT CONTROL SYSTEMS

John J. Burken*
NASA Dryden Flight Research Facility
P.O. Box 273
Edwards, California 93523-0273

Abstract

Singular value analysis can give conservative stability margin results. Applying structure to the uncertainty can reduce this conservatism. This paper presents flight-determined stability margins for the X-29A lateral–directional, multiloop control system. These margins are compared with the predicted unscaled singular values and scaled structured singular values. The algorithm was further evaluated with flight data by changing the roll-rate-to-aileron-command-feedback gain by ±20 percent. Minimum eigenvalues of the return difference matrix which bound the singular values are also presented. Extracting multiloop singular values from flight data and analyzing the feedback gain variations validates this technique as a measure of robustness. This analysis can be used for near-real-time flight monitoring and safety testing.

Nomenclature

Abbreviations

FFT	fast Fourier transform
GGS	ground-generated signal
MIMO	multiple-input–multiple-output
RDM	return difference matrix $[\mathbf{I} + \mathbf{HG}]$, $[\mathbf{I} + \mathbf{GH}]$
SISO	single-input–single-output
SSV	structured singular values
USV	unscaled singular values

Symbols

$\mathbf{A}$	general matrix
BLEND	blending table as a function of M, h, and α
$BMAX$	maximum yaw command, deg
$C1$, $C2$, $C3$	yaw command filter coefficients
$CFDP3$, $CFDP4$	roll command filter coefficients
$\mathbf{D}$	scaling matrix
$D1$, $D2$, $D3$	roll command filter coefficients
$\mathbf{e}$	actuating signal error vector
$\mathbf{GH}$	loop gain matrix
$\mathbf{G(s)}$	plant transfer function matrix
Ggs_δ_a	GGS telemetered from ground to aileron path
Ggs_δ_r	GGS signal telemetered from ground to rudder path
G_p	lateral stick gearing gain
g	acceleration caused by gravity, ft/sec^2
$\mathbf{HG}$	loop gain matrix
$\mathbf{H(s)}$, $\mathbf{H(z)}$	controller transfer function matrices, $z = \mathbf{e}^{sT}$
h	altitude, ft
I/O	input–output
$\mathbf{I}$	identity matrix
j	imaginary term, $j = \sqrt{-1}$
$K2$	roll-rate-to-aileron-feedback gain, deg/(deg/sec)
$K3$	yaw-rate-to-aileron-feedback gain, deg/(deg/sec)
$K4$	lateral-acceleration-to-aileron-feedback gain, deg/g
$K13$	lateral-stick-command-to-aileron gain, deg/percent

*Aerospace Engineer. Member AIAA.

$K14$	rudder-pedal-command-to-aileron gain, deg/percent
$K16$	roll-rate-to-rudder-feedback gain, deg/(deg/sec)
$K17$	yaw-rate-to-rudder-feedback gain, deg/(deg/sec)
$K18$	lateral-acceleration-to-rudder-feedback gain, deg/g
$K27$	lateral-stick-command-to-rudder gain, deg/percent
$K28$	rudder-pedal-command-to-rudder gain, deg/percent
k_i	structured uncertainty gain element of **L** matrix ($i = 1, n$)
L	perturbation matrix
$\mathbf{L_i}$	disturbance matrix at the input
$\mathbf{L_o}$	disturbance matrix at the output
M	Mach number
Ny	lateral acceleration, g
p	roll rate, deg/sec
r	yaw rate, deg/sec
$\mathbf{S_{uu}}$	autospectrum of input
$\mathbf{S_{xu}}$	cross spectrum of input-to-output
s	Laplace transform variable
T	sample period, 0.025 sec
t	time, sec
u	external input command vector
$VTRIM$	trim velocity, ft/sec
$\mathbf{X_u}$	control transfer function matrix
$XKI3$	roll forward-loop integrator gain
$XKP3$	roll forward-loop proportional gain
$XKP4$	yaw forward-loop proportional gain
x	control system output vector
y	plant output vector
z	Z-transform variable
α	angle of attack, deg
β	sideslip, deg
δ_a	aileron position
$\delta_a cmd$	aileron command to actuator, deg
δ_r	rudder position
$\delta_r cmd$	rudder command to actuator, deg
λ	eigenvalue
$\underline{\lambda}$	minimum eigenvalue
$\underline{\lambda}_{ANALY}$	analytical minimum eigenvalue
$\underline{\lambda}_{FLT}$	in-flight minimum eigenvalue
σ	singular values, $\sigma_n = \sqrt{\lambda_n(\mathbf{A}^*\mathbf{A})}$
$\bar{\sigma}$	maximum singular values
$\underline{\sigma}$	minimum singular values
$\underline{\sigma}_{FLT}$	in-flight minimum singular value
$\underline{\sigma}_{SSV}$	analytical SSV
$\underline{\sigma}_{USV}$	analytical USV
ϕ	roll attitude, deg
ϕ_i	structured uncertainty phase element of **L** matrix ($i = 1, n$)
ω	frequency, rad/sec
$\|\ \|$	Euclidean norm, 2 norm
$\|\ \|$	absolute value

Introduction

Multivariable control systems have been used for decades; however, the methodology to evaluate the stability margins was not developed until the last decade.[1] Classical frequency ω analysis methods, such as Bode or Nyquist techniques, work well for single-input–single-output (SISO) systems but are inadequate for multiple-input–multiple-output (MIMO) control systems. Classical methods do not allow for simultaneous variations of phase and gain in all of the feedback paths.[1–3] Recently, singular value σ norms of the return difference matrix (RDM) have been considered a measure of the system stability margin for multiloop feedback control systems.[1,2,4] However, singular value norms of systems with unstructured uncertainty can be overly conservative, and a control system designer could interpret the results as unsatisfactory when, in fact, the system is robust.[3] A method for relieving the excessive conservatism is derived by structuring the uncertainties.[2,3,5] A control system design is robust when it can perform well for substantial variations in plant dynamics.

Although mathematically sound, singular value methods require substantial evaluation using multiloop control systems before these methods can be accepted as adequate for determining the robustness of control system design. Some insight into application of experimentally determined singular values of a multiloop flutter suppression control system for a wind-tunnel aeroelastic model is presented in Ref. 6. In Ref. 6, singular values of the RDM at the input and output locations were used successfully to evaluate the performance of the control system. Reference 6 also gives computations for the open-loop transfer matrix **GH** from open-loop control system wind-tunnel operations. This reference concentrated on wind-tunnel aeroelastic control performance. Evaluation is also needed for unscaled

singular value (USV) and scaled structured singular value (SSV) methods for analyzing multiloop control systems of manned aircraft in flight. In addition, theoretical and flight-determined stability margins need to be compared.

To evaluate the stability of an in-flight multiloop system, the NASA Dryden Flight Research Facility conducted a flight test program on a MIMO flight control system using the X-29A aircraft (Grumman Aerospace Corporation, Bethpage, New York). The X-29A is an experimental aircraft designed to test the integration of several technologies. This aircraft was ideal for this study because the lateral–directional control system is multiloop with the capability of controlled excitation and measured response for MIMO analysis.[7]

This paper presents an extension of the evaluation method reported in Ref. 6 by determining singular values from flight data and comparing the values with the predicted or analytical USV and SSV, $\underline{\sigma}_{USV}$ and $\underline{\sigma}_{SSV}$. Flight results of the minimum eigenvalues $\underline{\lambda}$ obtained from the RDM and comparisons with the analytical minimum eigenvalues $\underline{\lambda}_{ANALY}$ are also presented. To determine the sensitivity of the MIMO stability margin algorithm, a lateral–directional X-29A control system feedback gain was changed during flight. Several flight conditions were flown and analyzed, but for the sake of brevity, one representative case is reported here. The flight test results are for three control law gain settings (80-, 100-, and 120-percent $K2$) at a flight condition of Mach number M 0.7 and an altitude h of 30,000 ft. The technique described in this paper can be used to obtain near-real-time stability margins during flight for multiloop control systems.

Test Vehicle Description

The X-29A is an experimental aircraft designed to test the feasibility of integrating several modern technologies into a highly maneuverable aircraft. This single-seat aircraft is powered by an F404-GE-400 engine (General Electric, Lynn, Massachusetts) with a thin supercritical 30° forward-swept wing and close-coupled canards. The wing contains full-span, double-hinged, trailing-edge flaperons which also provide variable camber. The wing structure includes aeroelastically tailored graphite-epoxy covers designed to provide stiffness to overcome the structural divergence problems associated with forward-swept wings. Figure 1 shows the X-29A aircraft. For a more complete description of the aircraft, see Refs. 7, 8, and 9.

Longitudinal control of the aircraft is achieved with canard, symmetric flaperons, and strake surfaces. The aircraft was designed with a high degree of longitudinal static instability, 35 percent at subsonic speeds. This instability requires the vehicle to be continuously stabilized by a fly-by-wire control system. Lateral–directional motion is controlled by a conventional rudder and differential flaperon deflection. The X-29A lateral–directional control system is multiloop and includes aileron-to-rudder and rudder-to-aileron interconnects for turn coordination.

Flight Control System Description

The X-29A aircraft has a triplex digital flight control system with an analog backup for each channel. The digital control law outputs are computed at 40 Hz in dual-processor flight computers. The primary task of the longitudinal control system is to stabilize the motion of the aircraft. Since the longitudinal flight control system is an SISO system, it is not evaluated in this report. The X-29A high angle-of-attack α, lateral–directional control system is multiloop. Figure 2 shows the major digital and dynamic elements. There are two pilot inputs: lateral stick and rudder pedal. The four aircraft feedback signals are roll rate p, yaw rate r, roll attitude ϕ, and lateral acceleration Ny. As Fig. 2 shows, seven paths are summed to generate the aileron command, including the ground-generated signal (GGS) command. Also, seven paths are summed for the rudder command, including the GGS command. The multiloop lateral–directional control and GGS systems, which can be summed to the actuated commands, make the X-29A ideal for MIMO stability analysis.

Roll-rate-to-aileron-feedback gain $K2$ is a function of flight condition. The $K2$ was the only gain that could be changed in flight that had any impact on the closed-loop stability margins. The $K2$ shown in Fig. 2 could only be changed by ±20 percent of the nominal value to determine the sensitivity of the singular value algorithm. The pilot could change the control system software $K2$ in flight by selecting a set of predetermined gains. The X-29A dynamics could also be excited by remote signals from a ground-based computer using the GGS system. For this study, the important control system is located at the input node where the signals are summed before being sent to the actuators (Fig. 2). The aileron-command-to-actuator $\delta_a cmd$ and rudder-command-to-actuator $\delta_r cmd$ signals are the resultant summed commands from the pilot, GGS, and control system feedback paths.

Ground-Generated Signal System Description

The X-29A flight control system was designed with the ability to remotely excite the aircraft dynamics with sweeps, step inputs, and doublets using a ground-based computer linked to the control system by telemetry transmission. The GGS system is used to repeat

maneuvers, provide for independent control surface inputs, and produce well-defined inputs for frequency response calculations.[9] Figure 2 shows that the GGS commands can be included in the aileron or rudder paths. For this analysis, the GGS consisted of a sinusoidal frequency sweep from 40.0 to 0.1 rad/sec. Refer to Ref. 9 for a more detailed discussion of the GGS system.

Data Acquisition System Description

The GGS, aileron, and rudder commands to the actuator are the only digital flight control system signals needed for this MIMO analysis. These signals were integrated with other data from a data bus and downlinked to the ground at 40 samples/sec. Figure 2 shows the GGS, aileron, and rudder commands to the actuator. The measured data were relatively noise free because the pilot inputs and feedback paths included antialiasing filters. For more information about the instrumentation, see Ref. 10.

Analytical Methods

Two methods of determining the analytical multivariable stability margins are discussed in this section. The two analytically determined robustness methods are referred to as USV and SSV.[3,5] The USV method can be too conservative, and the results could be interpreted as unsatisfactory stability margins when, in fact, these margins are adequate. The SSV method decreases the conservative nature of singular values. Structuring or scaling was not added to the flight-determined singular values because the flight data contains the complete system, including nonlinear and high-order system dynamic effects. The following subsections provide background information on stability margins using eigenvalues, flight data, and singular values as well as analytical structured and unscaled singular values.

Stability Margins Using Singular Values

Singular value analysis has been the focus of considerable interest in the controls discipline.[1-6,11] This analysis provides a way to determine how much uncertainty can be tolerated before a multivariable system becomes unstable and assumes that the system is initially stable. The singular values of the RDM are used to measure the stability margins.[1-4] The RDM at the input node is $[\mathbf{I} + \mathbf{HG}]$. At the output node, the RDM is $[\mathbf{I} + \mathbf{GH}]$. As the minimum singular value $\underline{\sigma}$ of the input or output RDM approaches zero, the system becomes increasingly less stable.

To analyze the RDM, a review of the general singular value analysis is helpful. Let $\mathbf{A}$ be a general $[n \times n]$ matrix, then the minimum and maximum singular values $\bar{\sigma}$ are

$$\underline{\sigma}[\mathbf{Ax}] = \min \| \mathbf{Ax} \| \equiv \sqrt{\lambda_{\min}[\mathbf{A}^*\mathbf{A}]} \quad \| \mathrm{x} \| = 1 \tag{1}$$

$$\bar{\sigma}[\mathbf{Ax}] = \max \| \mathbf{Ax} \| \equiv \sqrt{\lambda_{\max}[\mathbf{A}^*\mathbf{A}]} \quad \| \mathrm{x} \| = 1 \tag{2}$$

where $\| \mathbf{Ax} \|$ is the Euclidean norm; $\lambda[\mathbf{A}^*\mathbf{A}]$ are the eigenvalues; and $\mathbf{A}^*$ is the conjugate transpose of matrix $\mathbf{A}$. Note that the vector $\mathbf{Ax}$ depends on the units of the control system output vector $\mathbf{x}$ variables; therefore, the singular values also depend on the scale units of $\mathbf{x}$ variables.[2] Other useful properties of singular values are as follows:[2,3]

$$\underline{\sigma}[\mathbf{A}^{-1}] = 1/\bar{\sigma}[\mathbf{A}] \tag{3}$$

$$\underline{\sigma}[\mathbf{A}] \leq | \lambda[\mathbf{A}] | \leq \bar{\sigma}[\mathbf{A}] \tag{4}$$

Equation (4) states that the magnitude of the eigenvalues of $\mathbf{A}$ is bounded by the minimum and maximum singular values of $\mathbf{A}$.

Figure 3 shows a typical control system. The $\mathbf{G(s)}$ is the plant transfer function matrix, and $\mathbf{H(s)}$ is the control system transfer function matrix. Bold-faced variables, such as $\mathbf{G}$ and $\mathbf{H}$, are multiple path input and output matrices. The $\mathbf{L_i}$ and $\mathbf{L_o}$ represent the input and output perturbation matrices. The MIMO systems have cross-feed interactions which cause the locations of perturbations to impact the singular value results. In classical SISO systems, locations of the disturbances are unimportant. Ignoring the perturbation matrices for now, the relationships of the RDM for the input node $[\mathbf{I} + \mathbf{HG}]$ and the output node $[\mathbf{I} + \mathbf{GH}]$ are usually different. Therefore, the singular values are different because matrix multiplication is not commutative, i.e., $\mathbf{GH} \neq \mathbf{HG}$.

If the multiloop system is stable when unperturbed, then a sufficient but not necessary condition for the system to remain stable when $\mathbf{L_i}$ is perturbed is that[2,11,12]

$$\bar{\sigma}(\mathbf{L_i}^{-1} - \mathbf{I}) < \underline{\sigma}[\mathbf{I} + \mathbf{H}(j\omega)\mathbf{G}(j\omega)] \tag{5}$$

When analyzing the input node, the output perturbation matrix is set to identity, $\mathbf{L_o} = \mathbf{I}$. Likewise, the input perturbation matrix $\mathbf{L_i}$ is set to identity when analyzing the output node. The right-hand side of Eq. (5), $\underline{\sigma}[\mathbf{I} + \mathbf{HG}]$, is the minimum singular value of the input node RDM and is used as the basis of this robustness analysis. Analysis of singular values will work for SISO systems for determining stability margins.

Analytical Unscaled Singular Values

A fully populated perturbation matrix $\mathbf{L_i}$ produces the most conservative stability margins. The robustness of a system with a fully populated $\mathbf{L_i}$ can give an unrealistic measure of the stability margins.[1-3] Often,

these perturbations can be adequately defined using the diagonal elements of $\mathbf{L_i}$. When the $\mathbf{L_i}$ matrix is diagonal, it takes on the structure

$$\mathbf{L_i} = \mathrm{Diag}[k_1 e^{j\phi_1}, k_2 e^{j\phi_2} \ldots k_n e^{j\phi_n}] \qquad (6)$$

where k_i is the uncertainty gain element, and ϕ_i is the uncertainty phase element of the $\mathbf{L}$ matrix. Also, k_i and ϕ_i $(i = 1, n)$ may change independently and simultaneously with respect to one another in each control loop. This method allows for the robustness analysis of multivariable control systems.

Now that the ground work has been laid, the system stability boundary can be defined by testing the criterion

$$\underline{\sigma}[\mathbf{I} + \mathbf{HGL_i}(j\omega)] = 0 \qquad (7)$$

as a function of frequency. This expression is the neutral stability boundary that produces a pure resonance at ω. This relationship means that a pole of the closed-loop system on the imaginary axis exists. In addition, the minimum singular value of the RDM is zero. Whether the closed-loop system is stable or unstable, the singular values are always nonnegative as Eq. (1) indicates. The singular values are magnitudes of a transformation that are always positive and define the distance to the neutral stability boundary.[3] The reference for neutral stability is a minimum singular value of 0.0, and the stability margins are related to the magnitude of minimum singular value. The greater the magnitude of the minimum singular value, the greater the robustness.

One goal of this research was to extend the well-understood, classical stability margin methods from SISO to MIMO controllers. Equation (7) represents the information needed to determine the stability margins of a system. However in this form, this equation does not relate the magnitude of the minimum singular value to traditional phase and gain margins. The relationship that expresses the gain and phase as a direct function of either the input or output perturbations is shown in Eq. (8) and derived in Ref. 4, where $\mathbf{L}$ is either $\mathbf{L_i}$ or $\mathbf{L_o}$.

$$\sigma(\mathbf{L}^{-1} - \mathbf{I}) = \sqrt{\left(1 - \frac{1}{k_n}\right)^2 + \frac{2}{k_n}(1 - \cos(\phi_n))} \qquad (8)$$

Figure 4 shows a graphical representation of Eq. (8) and presents minimum singular value as a function of phase and gain margins. To determine the stability margins or nearness to instability, compute $\underline{\sigma}[\mathbf{I} + \mathbf{HG}(j\omega)]$ for various frequencies. The minimum singular value plot traces the nearness to singularity of the RDM and, thus, the system robustness to perturbations as a function of frequency. It is not necessary to know the perturbation matrix $\mathbf{L}$ to compute the minimum singular value plot. For more information regarding the stability boundary and its relationship to the perturbation matrix $\mathbf{L}$, see Ref. 3.

Analytical Scaled Structured Singular Values

Because the singular values of a fully populated $\mathbf{L}$-matrix are conservative, it may be misleading to apply these values to a control system. Such values may indicate that the system is not robust. The Analytical Unscaled Singular Values subsection structured the uncertainty by making the $\mathbf{L}$-matrix diagonal (see Eq. (6)). The USV method reduces the conservatism; however, scaling the system further reduces the conservatism. Scaling the system provides a way to reduce the conservatism and still maintain realistic margins.[1,3,5] This reduction is accomplished by including a diagonal scaling matrix $\mathbf{D}$ in the RDM expression. The scaling should be chosen so as to maximize the minimum singular value across the frequency range. Therefore, $\mathbf{D}(\omega)$ is a function of frequency, and the algorithms are easily implemented.[13]

$$\underline{\sigma}[\mathbf{I} + \mathbf{D}(j\omega)\{\mathbf{H}(j\omega)\mathbf{G}(j\omega)\}\mathbf{D}(j\omega)^{-1}] \leq \mathrm{SSV} \qquad (9)$$

Equation (9) represents the singular values as a function of frequency in the presence of the matrix $\mathbf{D}(\omega)$, which reduces the sensitivity of cross-feed perturbations. Implementation of the $\mathbf{D}$ matrix minimizes the conservative nature of singular values of multiloop robustness predictions. Equation (9) eliminates the conservatism for control systems where the dimension of $\mathbf{HG}$ is three or less.[5,11] Scaled singular values are the same as SSV and are used only for the analytical portion of the analysis. The predicted singular values of the RDM, $[\mathbf{I} + \mathbf{HG}]$ as well as $[\mathbf{I} + \mathbf{DHGD}^{-1}]$, can be determined from linear frequency analysis.

Eigenvalue Analysis

As shown in the Stability Margins Using Singular Values subsection, the node point location of the analysis can influence system stability. In addition, the singular values of the RDM can give a conservative measure of the closed-loop stability margins. Note that system singular values will always be upper bounded by the eigenvalues of the RDM, see Eq. (4). The eigenvalues of the RDM are identical at any location in the control system[6] and can be expressed as

$$\underset{\text{input node}}{|\,\underline{\lambda}(\mathbf{I} + \mathbf{HG})\,|} = \underset{\text{output node}}{|\,\underline{\lambda}(\mathbf{I} + \mathbf{GH})\,|} \qquad (10)$$

Equation (10) represents the upper limit of the minimum singular value and, therefore, the upper bounds of the stability margins of a multiloop control system. The eigenvalues of the RDM are not the same as those of the closed-loop system. As a reminder, closed-loop eigenvalues must be stable before applying this

stability margin analysis technique because minimum singular values only indicate how far from neutral stability the system is either stable or unstable.

Singular Value Analysis of Flight Data

The flight singular values and eigenvalues need to be determined by using frequency response techniques. This section describes the methodology used to determine singular values from flight test data. Transfer function equation development, eigenvalues, and singular values of the RDM are included.

A complex frequency response of a system can be estimated from the autospectrum and cross spectrum of the input and output time history variables by transforming these time domain responses to the frequency domain using fast Fourier transforms (FFT's). The controller input-to-output, $\{\mathbf{u}(t)\}$-to-$\{\mathbf{x}(t)\}$, transfer matrix (Fig. 3) $\mathbf{X_u}$ is defined as follows:

$$\{\mathbf{X_u}(j\omega)\}_{ij} = \sum_{l=1}^{N} (\mathbf{Sx}_j\mathbf{u}_i(j\omega))_l \{\mathbf{Su}_i\mathbf{u}_i(j\omega)_l\}^{-1} \quad (11)$$

where, $\mathbf{S_{xu}}$ is the cross spectrum of the input $\mathbf{u}$ and output $\mathbf{x}$. The $\mathbf{S_{uu}}$ is the autospectrum of the input, and N is the number of time history arrays. The data were loaded into arrays of 2048 points. A raised cosine smoothing window was used to process the time history data obtained from flight. See Ref. 8 for more details of the FFT procedures. The transfer functions produced by GGS excitation yielded good results.

Response matrix $\mathbf{X_u}$ can be used to construct the RDM $[\mathbf{I} + \mathbf{HG}]$. The following development shows the relationship of $\mathbf{X_u}$ to the RDM. Matrix terms $\mathbf{HG}$ or $\mathbf{GH}$ are called the loop gain matrices. Closed-loop system robustness is determined from the minimum singular values of the RDM at either the plant input node, $\underline{\sigma}[\mathbf{I} + \mathbf{HG}]$, or the output node, $\underline{\sigma}[\mathbf{I} + \mathbf{GH}]$. As the minimum singular values approach zero, the stability margin goes to zero. Perturbation matrices are not required for flight-determined singular value analysis because variations are inherent in the system dynamics. The following closed-loop relationships can be developed from Fig. 3 if the perturbation matrices are ignored:

$$\mathbf{e} = \mathbf{u} - \mathbf{x} \quad (12)$$

$$\mathbf{x} = \mathbf{HGe} = \mathbf{HG}[\mathbf{u} - \mathbf{x}] \quad (13)$$

The complex frequency response of the open-loop transfer function can be estimated from the autospectrum and cross spectrum of $\mathbf{u}$ and $\mathbf{x}$.

$$\mathbf{S_{xu}} = \mathbf{HG}[\mathbf{S_{uu}} - \mathbf{S_{xu}}] \quad (14)$$

This relationship can be postmultiplied by the autospectrum inverse $\mathbf{S_{uu}}^{-1}$.

$$\mathbf{S_{xu}S_{uu}}^{-1} = \mathbf{HG}[\mathbf{S_{uu}S_{uu}}^{-1} - \mathbf{S_{xu}S_{uu}}^{-1}] \quad (15)$$

Combining Eqs. (11) and (15) produces

$$\mathbf{X_u} = \mathbf{HG}[\mathbf{I} - \mathbf{X_u}] \quad (16)$$

Therefore, the loop gain matrix as a function of frequency is

$$\mathbf{HG}(j\omega) = \mathbf{X_u}(j\omega)[\mathbf{I} - \mathbf{X_u}(j\omega)]^{-1} \quad (17)$$

The response matrix $\mathbf{X_u}(j\omega)$ is square and has the dimensions equal to the number of inputs. The expressions have now been developed to determine the flight test singular values for the stability margins of multiloop control systems. The spectral relationships of this section can be rapidly evaluated using FFT's which make it possible to determine, during flight, the near-real-time stability margins of multiloop control systems.

Flight Test Procedure

The maneuvers flown for the multivariable stability margin analysis were designed to excite the motion of the lateral–directional axis. The pilot would stabilize the aircraft at the desired flight condition. Then, a GGS frequency sweep (Fig. 5) would be commanded to the roll axis to excite the X-29A dynamics. The GGS maneuver was complete after approximately 45 sec, and the pilot would reestablish the initial flight condition. Next, the same GGS frequency-sweep signal would be commanded to the yaw axis for approximately 45 sec to complete the needed inputs for the transfer function estimation. The GGS frequency-sweep signal started at 40 rad/sec and finished at 0.1 rad/sec. This type of signal sweep helped to maintain the initial flight condition without requiring pilot corrections. Ground-generated as well as aileron- and rudder-commands-to-actuator signals were recorded for the MIMO analysis at 40 samples/sec during the maneuvers. For the three $K2$ values, the pilot would dial in the appropriate settings on the control system panel, and the GGS maneuvers were repeated. The X-29A flight control system with its interconnects will not allow the pilot to generate independent controller excitation. Such excitation is essential for multiloop frequency analysis. As a result, pilot-commanded maneuvers were not used for this analysis.

Results and Discussion

This section presents flight results of singular values as a function of frequency and compares these results with the analytical USV and SSV. The minimum eigenvalues of the RDM and an evaluation of how the singular value analysis algorithm performed when a single gain in the feedback path was changed by ±20 percent are also presented. As mentioned in the Flight Control System Description section, $K2$ was the only gain that

could be changed easily in flight that had any impact on the stability margins. In addition, the flight conditions were $M = 0.7$ and $h = 30{,}000$ ft with $K2$ of 80, 100, and 120 percent of the nominal value.

The ground-generated input signals to the roll and yaw axes resulted in the response shown in Figs. 6 and 7. The robustness analysis for the X-29A was at the input node $[\mathbf{I} + \mathbf{HG}]$ and had two inputs (roll and yaw GGS commands) and two outputs (aileron and rudder commands to actuator). Therefore, the RDM dimension will be a 2×2 matrix that is a function of frequency.

Figure 8 shows the flight-determined input node minimum singular values, $\underline{\sigma}[\mathbf{I} + \mathbf{HG}]$, as a function of frequency with the nominal $K2$ as well as analytical structured and unscaled singular values. The plot shows that good agreement exists between the flight and analytical data. The analytical SSV's tend to agree slightly better with the flight data than the analytical USV's. This result is consistent with the theory. Figure 9 shows the scaling or structuring used on the analytical system for the nominal $K2$ maneuver. The dimension of the diagonal $\mathbf{D}$ is 2×2, which is the same size as $\mathbf{HG}$. The scaling algorithm set the $\mathbf{D}_{22}$ element to 1.0 and left the $\mathbf{D}_{11}$ element free to maximize Eq. (9). As shown in Fig. 9, $\mathbf{D}_{11}$ is the same order of magnitude as $\mathbf{D}_{22}$. Therefore, the scaling will not have as large an impact on the results as it would if the scaling were to differ by several orders of magnitudes. Another point to note is that as the $\mathbf{D}$ matrix approaches unity $\mathbf{I}$, the SSV's become the same as the USV's. Comparing the minimum singular values in Fig. 8 using scaling $\mathbf{D}$ elements in Fig. 9 shows that the modeling of the X-29A analytical system was good.

Obtaining good low-frequency results is difficult when the flight maneuver is time limited (45 sec for this analysis) because several periods at a given frequency may be needed to accurately define the transfer function. The X-29A flight data transfer functions were truncated below 0.9 rad/sec because of increasingly poor transfer function definition. However, the important location on a singular value plot is the global minimum singular value, which is 0.72 at 8.0 rad/sec (Fig. 8), because this represents the worst closed-loop stability margin. The universal phase and gain margin plot of Fig. 4 is required to relate the $\underline{\sigma} = 0.72$ to a stability margin. From Fig. 4, a singular value of 0.72 corresponds to gain margins of -4.8 and 11.5 dB and to a phase margin of $\pm 41°$. The dashed lines highlight the area of interest in this figure. These singular values thus imply that the gain in both paths can be increased by 11.5 dB or reduced by 4.8 dB simultaneously before the system becomes unstable. Similarly, the phase in both paths can be changed by $\pm 41°$ before the system becomes unstable. Flight and analytical scaled global minimum singular values are close to each other. The analytical unscaled global minimum singular value is approximately 0.65 at 8 rad/sec, which corresponds to a gain margin between -4 and 8.5 dB and a phase margin of $\pm 35°$. The SSV method matched the peak and valley of the flight minimum singular values better than the USV method. As expected, the analytical USV stability margins were lower or more conservative than the analytical SSV margins.

Figure 10 shows the minimum eigenvalue as a function of frequency of the RDM $[\mathbf{I} + \mathbf{HG}]$. Minimum analytical eigenvalues compare very well with the flight-determined RDM eigenvalues. The eigenvalues are invariant under scale changes (as mentioned in the Eigenvalue Analysis subsection (Eq. (10))). The minimum eigenvalue is the upper bound of the minimum singular value of the RDM, as expressed in Eq. (4). Figure 11 combines the flight-determined minimum eigenvalue from Fig. 10 and the minimum singular value from Fig. 8. The singular value curves are equal to or below the eigenvalue curve which agrees with Eq. (4) $[\underline{\sigma} \leq \underline{\lambda}]$. Analytical USV's are not presented.

To investigate the ability of the algorithm to detect a change in stability margins, $K2$ was changed in flight by ± 20 percent, and the same flight maneuvers were performed again. Figure 12 shows the results for $K2$ of 80 percent of the nominal value flown at $M = 0.7$ and $h = 30{,}000$ ft. Figure 13 shows the results for $K2$ of 120 percent of the nominal value. The analytical USV's are generally lower than the flight singular values and are always less than or equal to the SSV's. The SSV curve compares well with the in-flight values at the lower frequencies. In addition, the USV and SSV are in close agreement at the minimum singular values location. For comparison, Fig. 14 shows the three flight-determined singular values for the three $K2$ settings: 80, 100, and 120 percent. The algorithm detected the multiloop stability margin change caused by the single $K2$ change of ± 20 percent.

Since the analytical results matched the flight results very well, it can be concluded that the flight minimum singular value can be used as a measure of multiloop stability margins. Although the near-real-time analysis was not done in this report, the time used to generate flight-determined minimum singular value was less than 30 sec and is considered insignificant. The size of the RDM $[\mathbf{I} + \mathbf{HG}]$ was $2 \times 2 \times 1024$ frequencies. These computation times are small enough to support near-real-time, multiloop stability margin analysis. The near-real-time capability would minimize the time required for envelope expansion of aircraft with multiloop control systems.

Concluding Remarks

Multiloop stability margins were determined for the X-29A aircraft from flight data using the methods presented in this paper. The flight results compared well with predicted stability margins. Analytical stability robustness was determined using unscaled and scaled structured singular value analyses. The flight-determined singular values were determined using the closed-loop frequency responses. Data analysis comparing predictions of both methods showed good correlation. However, the scaled structured singular value method matched the flight minimum singular value better at the lower frequencies. The predicted unscaled singular value minimums were always conservative compared with the scaled structured singular values throughout the entire frequency range. Predicted and flight-determined minimum eigenvalues of the return difference matrix were also presented. Sensitivity of the algorithm was evaluated by changing a feedback gain by ±20 percent, and the stability margins were compared with the nominal gain results. The analysis method is suitable for detecting changes in stability margins.

Extracting multiloop singular values from flight data and comparing the information with prediction validates the application of the technique as a relative measure of robustness. This comparison increases the confidence of using singular values for stability assessments of multiloop control systems. The technique described in this report can be used on any multiloop control system. Also, this technique extends the single-loop gain and phase margin concepts to multiloop systems. The methodology could be implemented in near real time for flight-monitoring and safety requirements. Near-real-time capability would minimize the time required for envelope expansion of aircraft with multiloop control systems.

References

[1]Doyle, John C. and Gunter Stein, "Multivariable Feedback Design: Concepts for a Classical/Modern Synthesis," *IEEE Trans. Automat. Contr.*, vol. AC-26, no. 1, Feb. 1981, pp. 4–16.

[2]Ly, Uy-Loi, "Robustness Analysis of a Multiloop Flight Control System," AIAA-83-2189, Aug. 1983.

[3]Paduano, James D. and David R. Downing, *Application of a Sensitivity Analysis Technique to High-Order Digital Flight Control Systems*, NASA CR-179429, 1987.

[4]Newsom, Jerry R. and V. Mukhopadhyay, "A Multiloop Robust Controller Design Study Using Singular Value Gradients," *J. Guidance, Control, and Dynamics*, vol. 8, no. 4, July–Aug. 1985, pp. 514–519.

[5]Doyle, John C., Joseph E. Wall, and Gunter Stein, "Performance and Robustness Analysis for Structured Uncertainty," *Proc. 21st IEEE Conference on Decision and Control*, vol. 2, Dec. 1982, pp. 629–636.

[6]Pototzky, Anthony S., et al., *Development and Testing of Methodology for Evaluating the Performance of Multi-Input/Multi-Output Digital Control Systems*, NASA TM-102704, 1990.

[7]Gera, J., J.T. Bosworth, and T.H. Cox, *X-29A Flight Test Techniques and Results: Flight Controls*, NASA TP-3121, 1991.

[8]Bosworth, John T., *Flight-Determined Longitudinal Stability Characteristics of the X-29A Airplane Using Frequency Response Techniques*, NASA TM-4122, 1989.

[9]Clarke, Robert, et al., *Development and Flight Test of the X-29A High Angle-of-Attack Flight Control System*, NASA TM-101738, 1991.

[10]Sefic, Walter J. and Cleo M. Maxwell, *X-29A Technology Demonstrator Flight Test Program Overview*, NASA TM-86809, 1986.

[11]Mukhopadhyay, V. and J.R. Newsom, "Application of Matrix Singular Value Properties for Evaluating Gain and Phase Margins of Multiloop Systems," AIAA-82-1574, Aug. 1982.

[12]Paduano, James D. and David R. Downing, "Sensitivity Analysis of Digital Flight Control Systems Using Singular-Value Concepts," *J. Guidance, Control, and Dynamics*, vol. 12, no. 3, May–June 1989, pp. 297–303.

[13]Thompson, Peter, "Note on Multivariable Gain and Phase Margins," California Institute of Technology, Pasadena, California, Mar. 1986.

ORIGINAL PAGE
BLACK AND WHITE PHOTOGRAPH

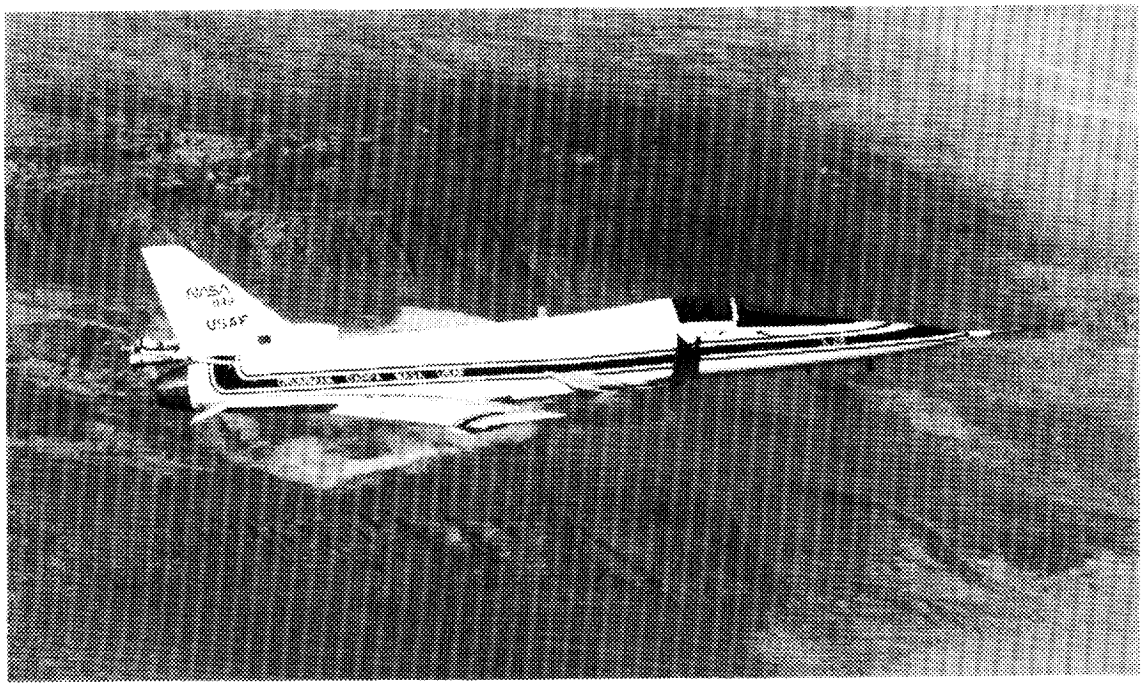

EC 90 48-17

Fig. 1 The X-29A aircraft.

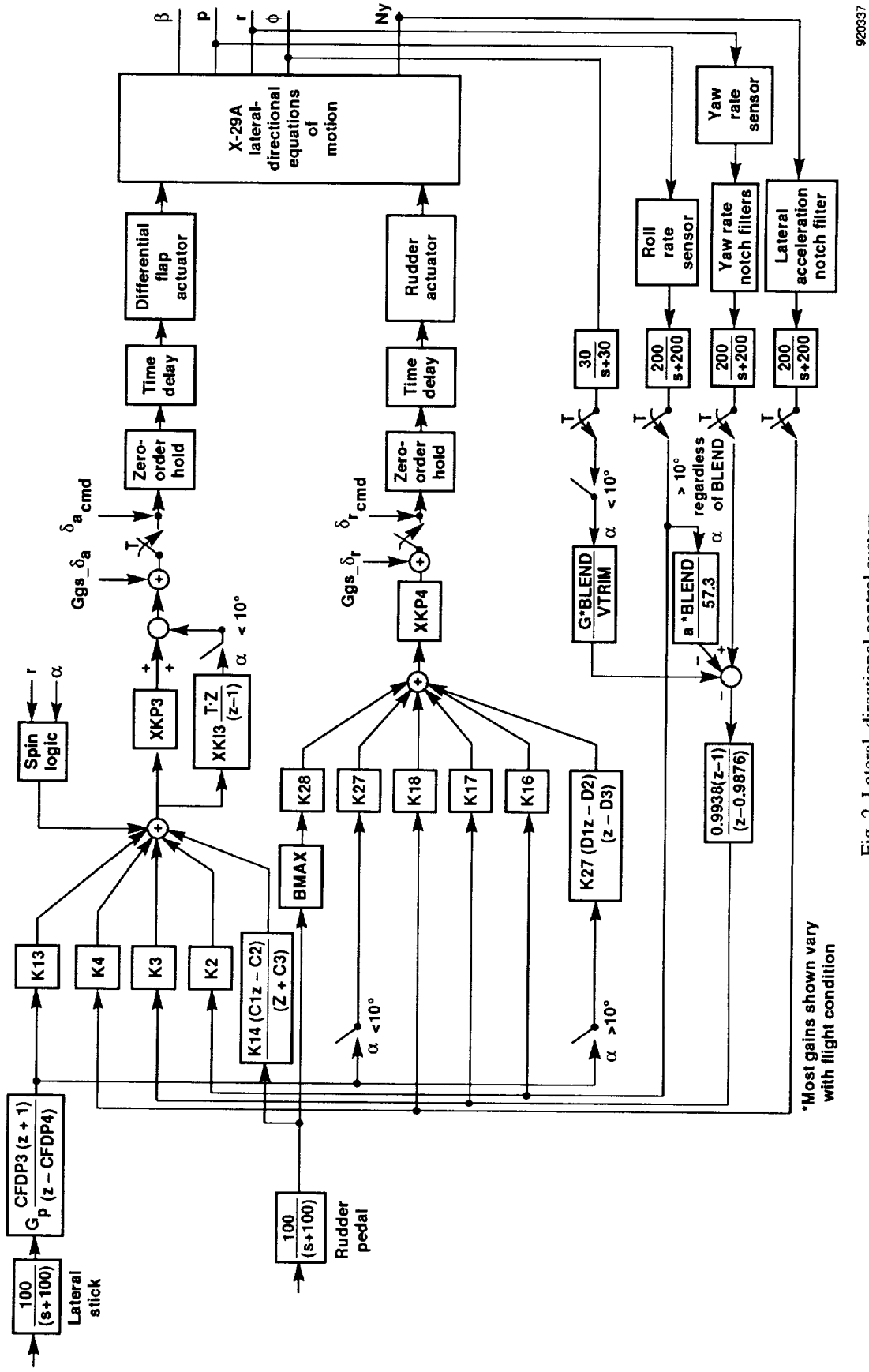

Fig. 2 Lateral–directional control system.

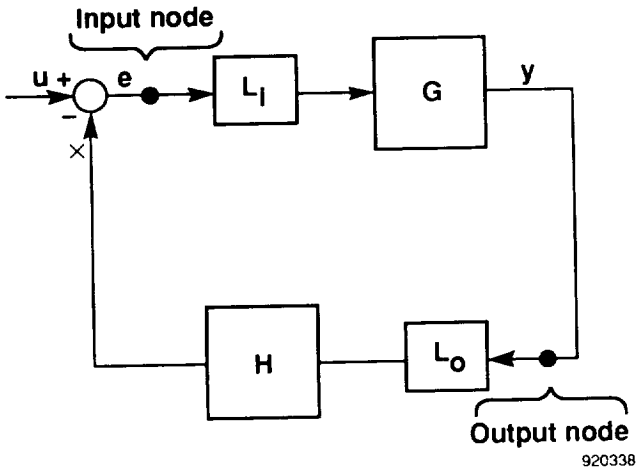

Fig. 3 Control system diagram with disturbance matrices at the input and output nodes.

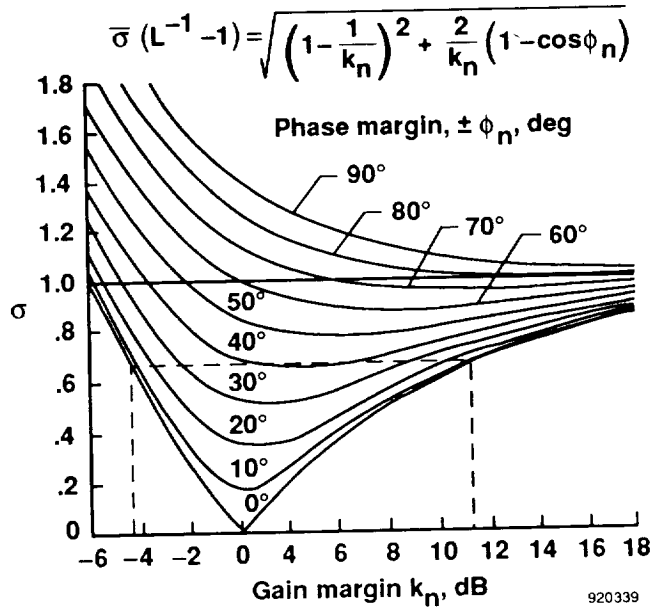

Fig. 4 Universal diagram for multiloop gain-phase margin evaluation.

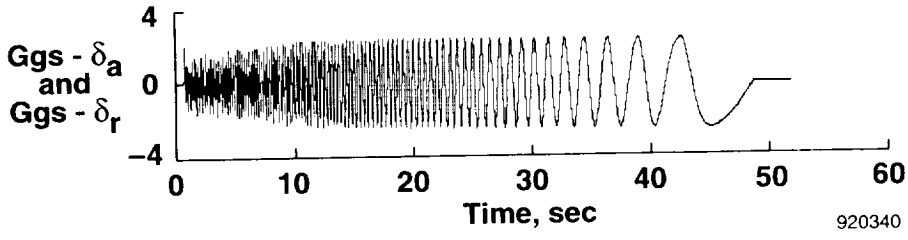

Fig. 5 The ground-generated signal frequency-sweep input for roll and yaw axes.

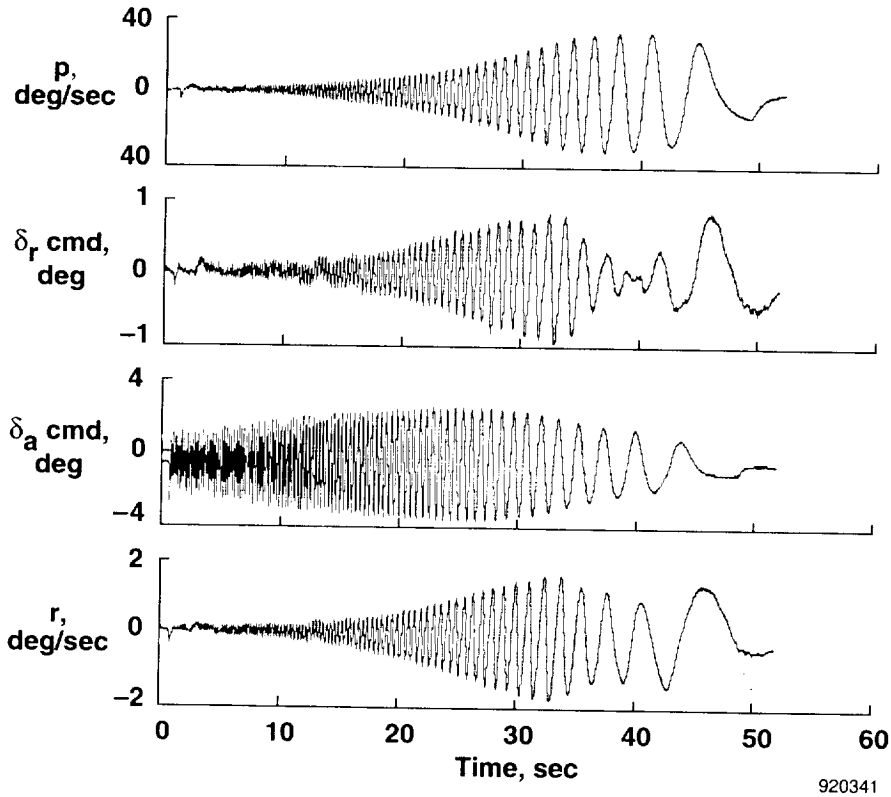

Fig. 6 Roll axis frequency-sweep time histories caused by ground-generated signals telemetered from the ground to the aileron-path input for a Mach number of 0.7, an altitude of 30,000 ft, and a roll-rate-to-aileron-feedback gain of 100 percent.

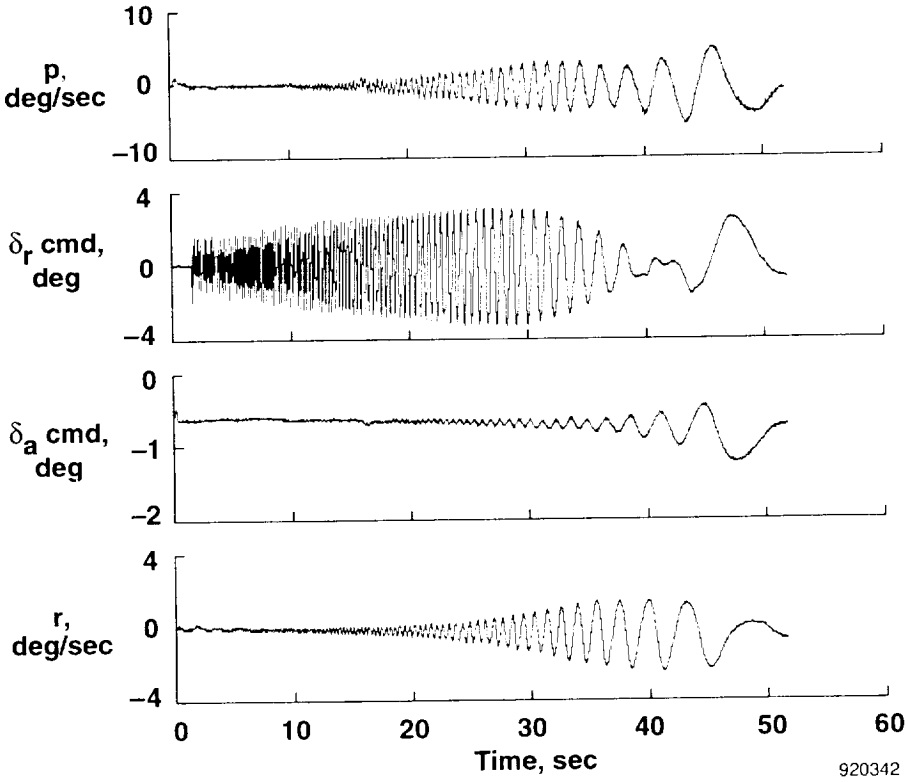

Fig. 7 Yaw axis frequency-sweep time histories caused by ground-generated signals telemetered from the ground to the rudder-path input for a Mach number of 0.7, an altitude of 30,000 ft, and a roll-rate-to-aileron-feedback gain of 100 percent.

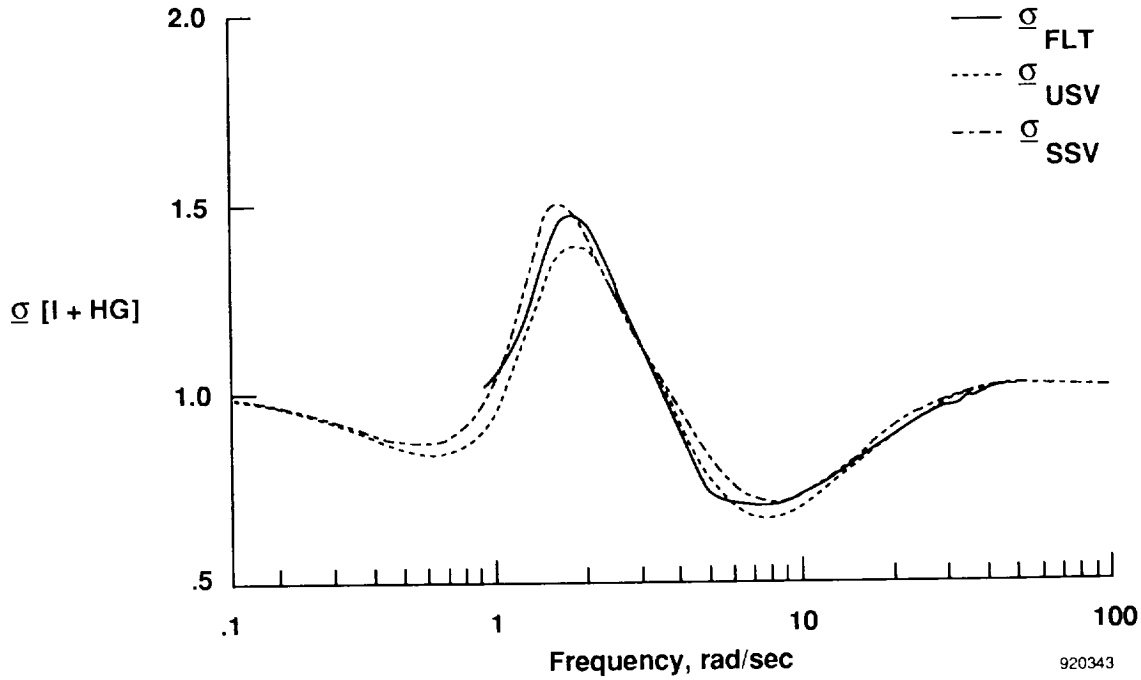

Fig. 8 Flight and predicted minimum singular values as a function of frequency for a Mach number of 0.7, an altitude of 30,000 ft, and a roll-rate-to-aileron-feedback gain of 100 percent.

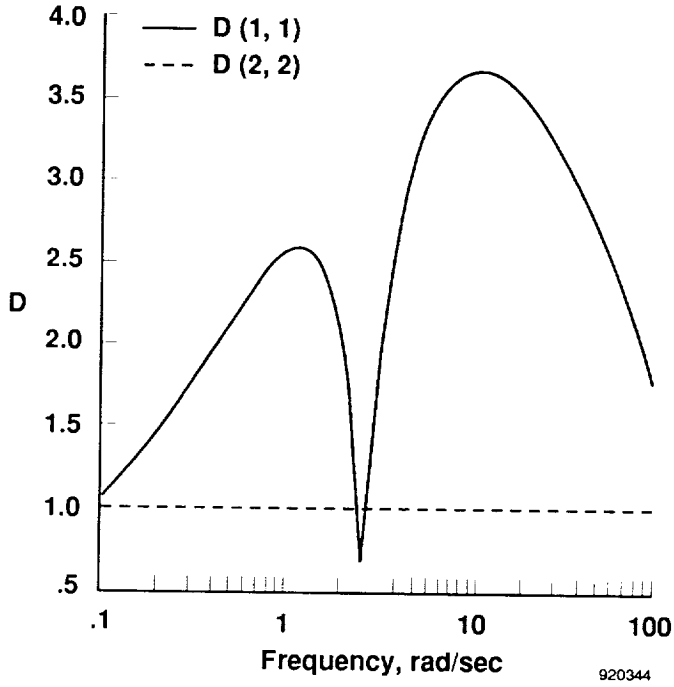

Fig. 9 Diagonal scaling matrix $\mathbf{D}(\omega)$ applied to the input return difference matrix for a Mach number of 0.7, an altitude of 30,000 ft, and a roll-rate-to-aileron-feedback gain of 100 percent.

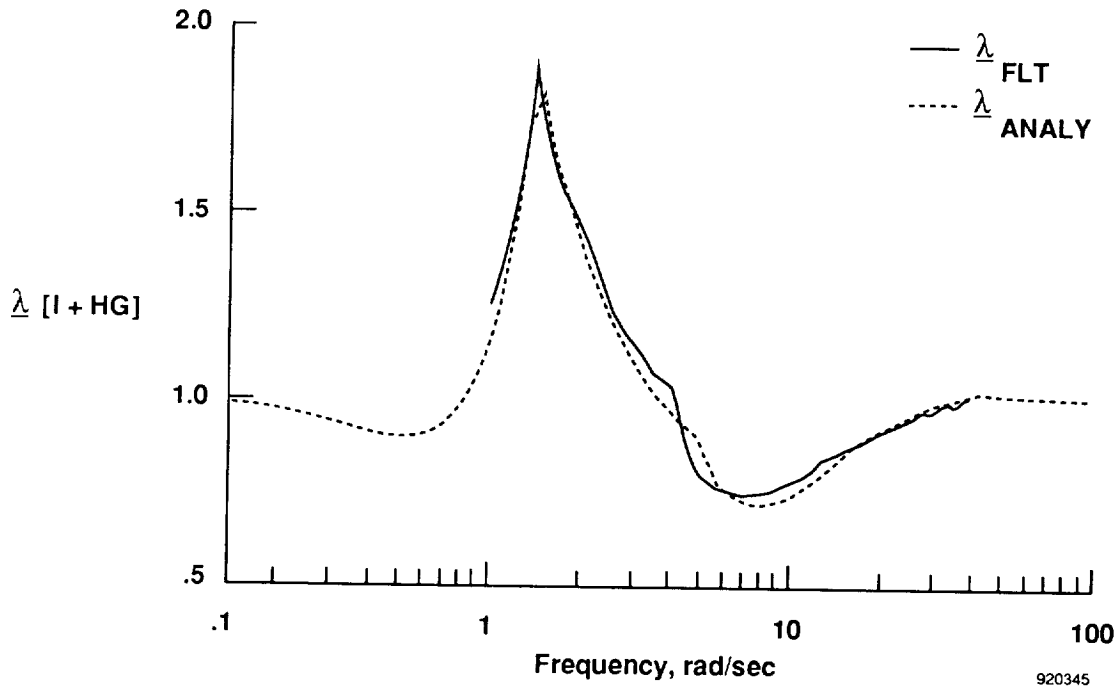

Fig. 10 Flight and predicted minimum eigenvalues of $[\mathbf{I} + \mathbf{HG}]$ for a Mach number of 0.7, an altitude of 30,000 ft, and a roll-rate-to-aileron-feedback gain of 100 percent.

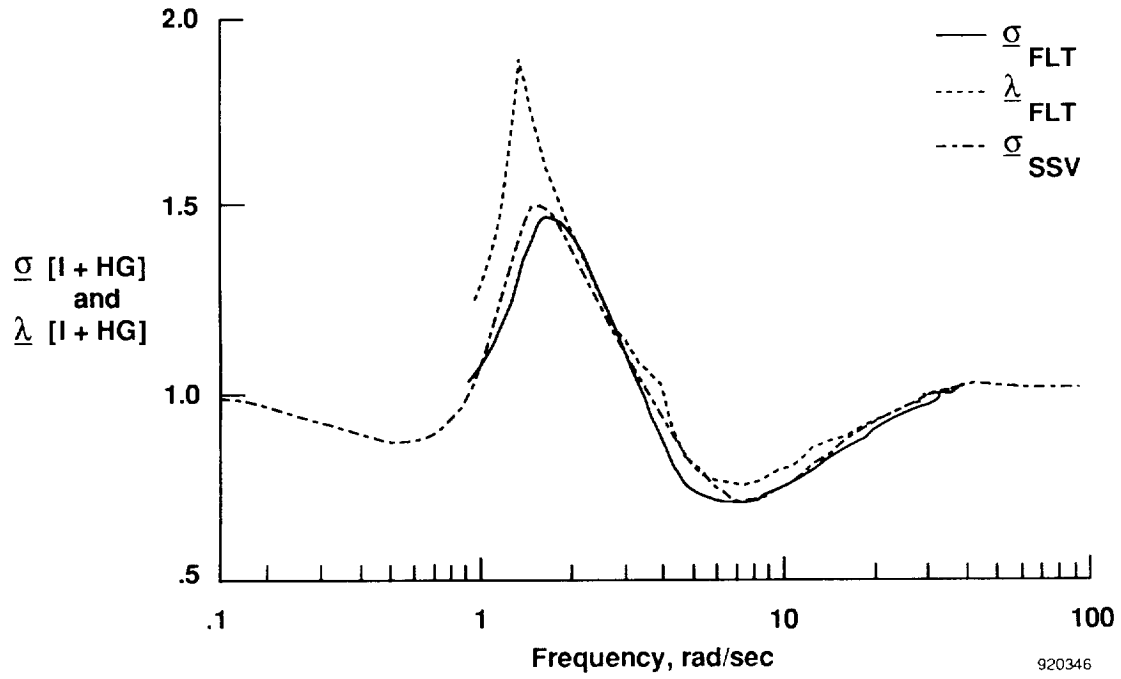

Fig. 11 Flight and predicted minimum singular values and eigenvalues of $[\mathbf{I} + \mathbf{HG}]$ for a Mach number of 0.7, an altitude of 30,000 ft, and a roll-rate-to-aileron-feedback gain of 100 percent. Note that $\sigma_{\min}[\mathbf{I} + \mathbf{HG}] \leq |\lambda_{\min}[\mathbf{I} + \mathbf{HG}]|$.

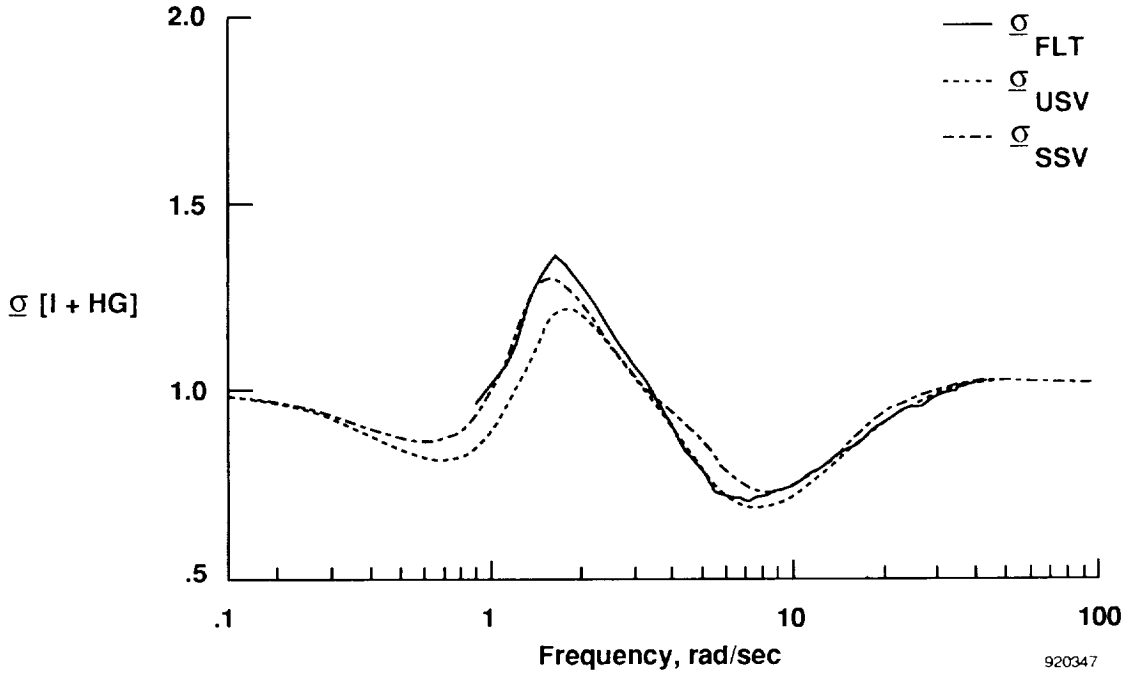

Fig. 12 Flight and predicted minimum singular values of $[\mathbf{I} + \mathbf{HG}]$ for a Mach number of 0.7, an altitude of 30,000 ft, and a roll-rate-to-aileron-feedback gain of 80 percent.

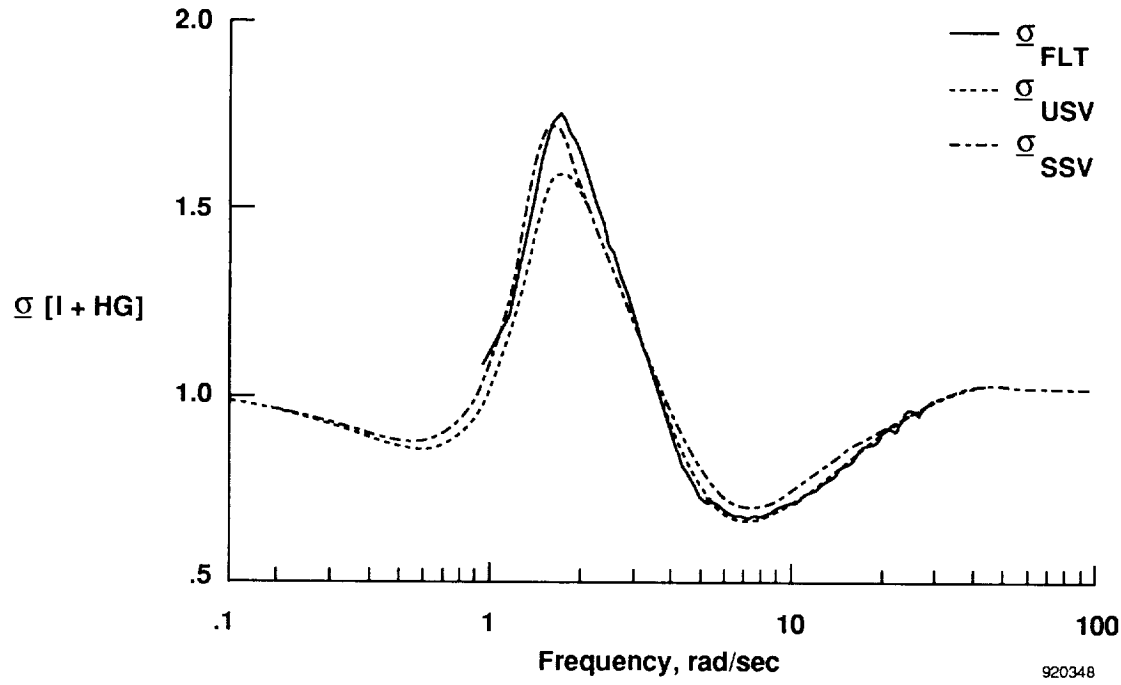

Fig. 13 Flight and predicted minimum singular values of input node [I + HG] for a Mach number of 0.7, an altitude of 30,000 ft, and a roll-rate-to-aileron-feedback gain of 120 percent.

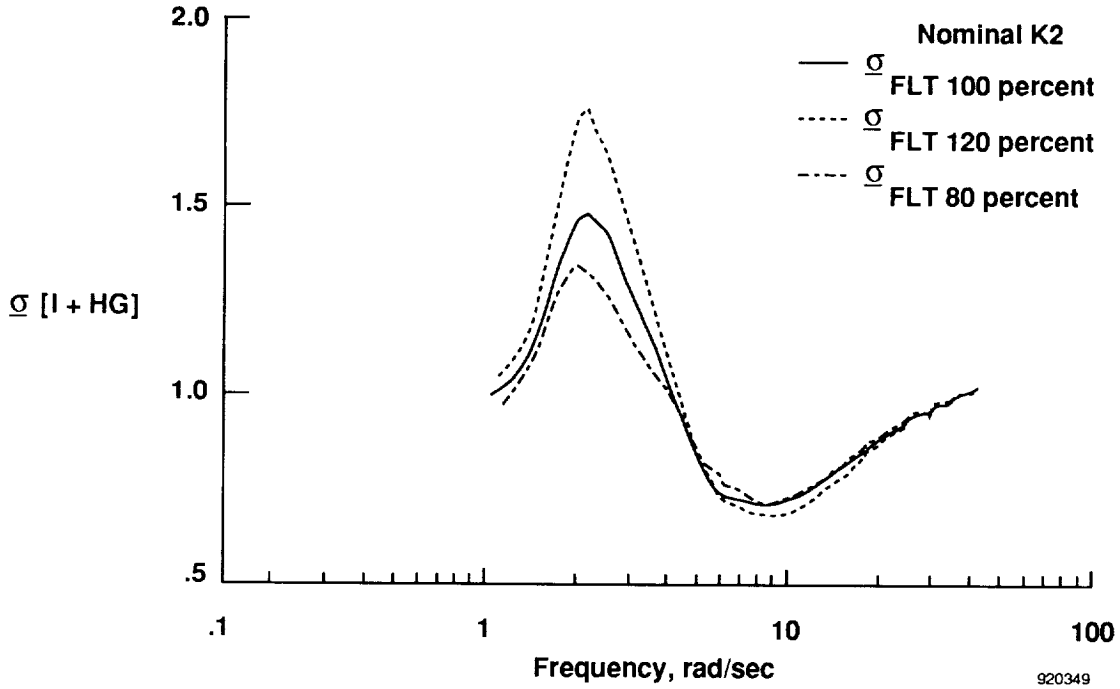

Fig. 14 Flight minimum singular values as a function of gain settings for a Mach number of 0.7, an altitude of 30,000 ft, and a roll-rate-to-aileron-feedback gain of 120, 100, and 80 percent.